Energy Equip. Sys./ Vol. 11/No. 3/September 2023/ 261-275

ENERGY EQUIPSYS

Energy Equipment and Systems

http://energyequipsys.ut.ac.ir

www.energyequipsys.com

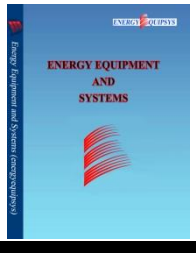

Thermodynamic analysis of a combined ORC and ejector vapor compression refrigeration system utilizing a PEMFC

Author

Armin Emamifar[a*]

[a]Mechanical Engineering Department, Ayatollah Boroujerdi University, Boroujerd, Iran

Article history:

Received :8 December 2022
Accepted : 28 May 2023

ABSTRACT

In this study, thermodynamic analysis for integration of a PEMFC with an organic Rankin cycle, and an ejector expansion vapor compression refrigeration system is presented. The input energy of the system is supplied by the waste heat of a PEMFC. Energy and exergy analysis is performed on each system component and compared with a simple ORC-VCR without an ejector. The results show that employing the ejector can improve the refrigeration capacity, energy efficiency, and exergy efficiency by 18.88%, 12.29 %, and 12.27%, respectively, compared to a simple ORC-VCR system. Moreover, the overall energy and exergy efficiency of the system is 33.43% and 5.46% higher than a standalone PEM fuel cell. Furthermore, in the parametric study, the effect of condenser temperature, evaporator temperature, ejector efficiency, PEMFC operating temperature, current density, and PEMFC operating pressure on the energy efficiency, exergy efficiency, and refrigeration capacity of the system is investigated.

Keywords: PEMFC; ORC; VCR; Ejector; Exergy Analysis.

1. Introduction

The depletion of fossil fuels and environmental and economic problems are the main concerns in thermal systems [1-3]. In this regard, many efforts have been carried out to enhance the performance of the systems. Utilizing various forms of renewable energies such as wind, solar, geothermal, biomass, hydrogen, and waste heat has been given more attention in recent years [4]. Among various power systems, the organic Rankine cycle (ORC) indicates better performance in low and medium operating temperatures. By integrating an ORC with a vapor compression refrigeration cycle, a thermally activated cooling system can be achieved. On the other hand, using a two-phase ejector in the vapor refrigeration systems can increase its performance. An ejector that has no moving part, simple structure, and low cost can increase the COP of a refrigeration system by reducing the throttling losses and compressor work [5-7]. Therefore, combining an ORC with an EERC can provide better performance for converting low-grade waste heat to electricity or cooling [8]. This combination can achieve its energy from a renewable heat source. Fuel cells can convert the chemical energy of fuels to electrical energy, water, and heat. Much research has been done on using the waste heat of fuel cells in various systems [9-29]. The ORC-EERC can

* Corresponding author: Armin Emamifar
Mechanical Engineering Department, Ayatollah Boroujerdi University, Boroujerd, Iran
Email: emamifar@abru.ac.ir

attain its input energy from the waste heat of a PEM fuel cell. Several studies have been carried out to investigate the performance of the ORC-VCR systems. Aphornatana and Sirveerakul [30] analyzed an ORC-VCR system operated by low-grade thermal energy. They used R22 and R134a as working fluids and revealed that R22 has a better COP than R134a. Wang et al. [31] combined an ORC with a vapor compression refrigeration system to provide cooling from the waste heat of engines. Li et al. [32] compared the performance of an ORC-VCR system for different hydrocarbon working fluids including butane, propane, propylene, and isobutene. They demonstrated that butane has better performance. Li et al. [33] proposed a combined power-refrigeration system using flue gas as the heat source and investigated the effect of condensation temperature, flue gas temperature, and turbine inlet pressure on the system efficiency. Saleh [34, 35] evaluated different working fluids to use in an ORC-VCR system in low-grade thermal power plants and carried out a parametric study based on effective thermodynamic parameters of the system. Zheng et al. [36] used zeotropic mixtures in a solar ORC-VCR system including an internal heat exchanger in the ORC cycle and compared the performance of eight pure fluid and five zeotropic mixtures. Ashwni et al. [37] proposed a modified ORC-VCR system containing an additional compressor, flash tank, and expansion valve. They used the zeotropic mixture as a working fluid and concluded that the proposed system can provide better energetic, exergetic, and economic performance. Bao et al. [38] investigated four different combined ORC-VCC and ORC-FTVIC systems based on single fluid and dual fluid. They employed geothermal energy as the heat source and demonstrated that dual fluid systems provide higher cooling capacity. Ghorbani et al. [39] used the waste heat of an internal combustion engine in a cogeneration system to provide refrigeration. They reported that R600 and R245fa show better performance in the system. Karellas and Braimakis [40] proposed a cogeneration system based on solar energy and biomass fuel to produce power, heat, and refrigeration. They investigated the system performance for summer and winter operations. Kim and Blanco [41] studied the use of eight different working fluids in an ORC-VCC system powered by a low-grade heat source. They also investigated the effect of key parameters on the performance of the system.

Integrating ORC-VCR systems with low-grade energy sources is a certain technique to achieve higher system efficiencies. To the best author's knowledge, the combination of an ORC-VCR and a PEM fuel cell has not been reported in the literature. In the present study, to obtain the best results, a novel hybrid system for producing power and refrigeration that takes advantage of a PEM fuel cell and an ejector expansion device is proposed. The waste heat of the fuel cell is recovered by the ORC-VCR. Besides, the use of the ejector increases the refrigeration capacity of the system. Energy and exergy analysis of the system is investigated and the results have been compared with a simple ORC-VCR system without the ejector. Moreover, the effect of fuel cell pressure, current density, condensation temperature, and evaporator temperature on the system's performance is studied and the energy and exergy efficiencies are evaluated.

2. System description

The schematic diagram of the proposed hybrid system consisting of a PEM fuel cell, an ORC, and an ejector VCR cycle (PEM-ORC-EVCR) is displayed in Fig.1. Hydrogen and air enter the fuel cell to generate power after an electrochemical reaction. The output streams are water and air. The unreacted hydrogen returns to the fuel cell inlet. A considerable amount of heat is also generated through the reactions in the fuel cell which is used as the heat source for the ORC-EVCR combined cycle to produce power and refrigeration. The ORC-EVCR cycle consists of a vapor generator, a turbine, a condenser, a pump, an expansion valve, an ejector, and an evaporator. The saturated liquid exiting the condenser splits into two parts. A part of it is pumped to the vapor generator to receive heat from the PEM fuel cell and evaporates to saturated vapor. The outlet of the vapor generator enters the turbine to produce

work and then flows to the condenser. The other part of the condenser outlet enters the ejector nozzle as the primary fluid which expands into low-pressure and high-velocity fluid to entrain the outlet vapor of the evaporator (secondary fluid). After mixing the primary and secondary fluids in the mixing chamber, the mixed fluid flows to the diffuser and, its pressure increases. The outlet stream of the ejector which is in a phase state enters the separator. Then the saturated liquid passes through the expansion valve and enters the evaporator. The saturated vapor outlet of the separator flows to the compressor, where it compresses to the condenser pressure. Then it mixes with the turbine outlet and enters the condenser.

3. Thermodynamic modeling

The thermodynamic simulation of the proposed system is presented in this section. The following assumptions are considered in the thermodynamic modeling of the system:

- The system operates at a steady state.
- The isenthalpic process is considered in the expansion valve.
- The pressure losses in the pipes and heat exchangers are neglected.
- The chemical reactions in the fuel cell reach equilibrium.
- Constant pressure is assumed in the fuel cell.
- The air composition in the fuel cell is 79% N_2 and 21% O_2.
- The fully saturated condition is assumed at the interface of the cathode and membrane.
- The isentropic efficiency of the turbine, pump, and compressor are considered 0.85, 0.9, and 0.8, respectively.

The electrochemical reactions occurring in the PEM fuel cell are as follows:

$$Anode: H2 \rightarrow 2H^{+} + 2e^{-} \quad (1)$$

$$Cathode: 2H^{+} + 2e^{-} + 0.5O_2 \rightarrow H_2O \quad (2)$$

$$Overall: H_2O + 0.5O_2 \rightarrow 2H_2O \quad (3)$$

The power generated in the fuel cell can be expressed as follows:

$$W_{fc} = N_{Cell} V_{fc} I \quad (4)$$

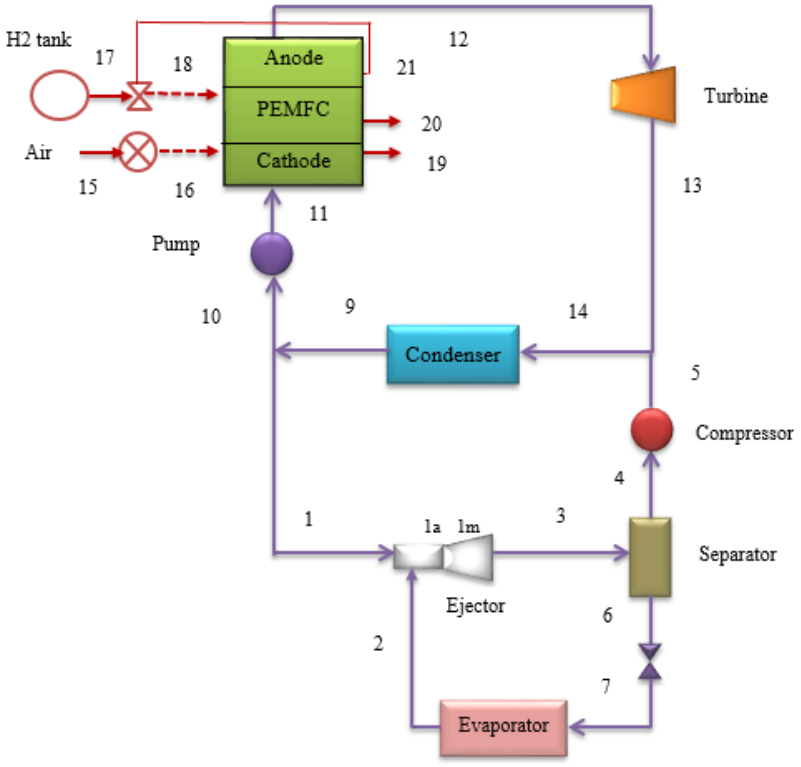

Fig. 1. Schematic diagram of the proposed PEM-ORC-EVCR system

where, N_{cell} is the number of cells in the stack, I is the current and V_{fc} denotes the actual voltage of the cells. The actual fuel cell voltage can be obtained using the following equation:

$$V_{fc} = E_{Nernst} - V_{act} - V_{ohm} - V_{conc} \tag{5}$$

where E_{Nernst} is the open circuit voltage in the fuel cell and is defined as follows:

$$E_{Nernst} = \frac{-\Delta G^0}{n_e F} + \frac{RT_{fc}}{n_e F} \ln\left(\frac{P_{H_2}\left(P_{O_2}\right)^{0.5}}{P_{H_2O}^{sat}}\right) \tag{6}$$

where P_{H2} and P_{O2} are partial pressures of hydrogen and oxygen in the fuel cell.

$$P_{H_2} = 0.5 P_{H_2O}^{sat}\left[\frac{1}{\exp\left(1.653 i / T_{fc}^{1.334}\right).x_{H_2O}^{sat}} - 1\right] \tag{7}$$

$$P_{O_2} = P\left[1 - x_{H_2O}^{sat} - x_{N_2}^{channel}\exp\left(0.291 i / T_{fc}^{0.832}\right)\right] \tag{8}$$

where P is the PEM fuel cell operating pressure, $x_{N_2}^{channel}$ is the molar fraction of nitrogen, I is the current density, $x_{H_2O}^{sat}$ is the mole fraction of saturated vapor water in the gas stream and $P_{H_2O}^{sat}$ is the partial pressure of vapor water.

$$\begin{aligned}\log\left(P_{H_2O}^{sat}\right) &= -2.1794 + 0.02953\left(T_{fc} - 273.15\right) \\ &-9.1837\times10^{-5}\left(T_{fc} - 273.15\right)^2 + 1.4454\times10^{-7}\left(T_{fc} - 273.15\right)^3\end{aligned} \tag{9}$$

where $x_{N_2,in}$ and $x_{N_2,out}$ denote the molar fraction of nitrogen in the inlet and outlet streams. Furthermore, λ_{air} represents the air stoichiometric rate.

$$x_{N_2}^{channel} = \frac{\left(x_{N_2,in} - x_{N_2,out}\right)}{\ln\left(\frac{x_{N_2,in}}{x_{N_2,out}}\right)} \tag{10}$$

$$x_{N_2,in} = 0.79\left(1 - x_{H_2O}^{sat}\right) \tag{11}$$

$$x_{N_2,out} = \frac{1 - x_{H_2O}^{sat}}{1 + \left(\left(\lambda_{air} - 1\right)/\lambda_{air}\right)\left(0.21/0.79\right)} \tag{12}$$

The activation over potential is due to the reduction of the reactions occurring on the electrode surfaces and can be obtained as follows:

$$\begin{aligned}V_{act} = -\Big[&-0.948 + \xi T_{fc} - 0.000193 T_{fc}\left(\ln\left(C_{O_2,conc}\right)\right) \\ &+0.000076 T_{fc}\left(\ln(I)\right)\Big]\end{aligned} \tag{13}$$

$$\xi = 0.00286 + 0.0002\ln\left(A_{cell}\right) + 0.000043\ln\left(C_{H_2,conc}\right) \tag{14}$$

where A_{cell} is the surface area, $C_{H_2,conc}$ represents the hydrogen concentration at the cell anode membrane interface, and $C_{O_2,conc}$ denotes the oxygen concentration at the fuel cell cathode membrane interface.

$$C_{O2,conc} = 1.97\times10^{-7} P_{O_2}\exp\left(\frac{498}{T_{fc}}\right) \tag{15}$$

$$C_{H_2,conc} = 9.174\times10^{-7} P_{H_2}\exp\left(\frac{-77}{T_{fc}}\right) \tag{16}$$

The Ohmic overvoltage is calculated based on Ohm's law:

$$V_{ohm} = IR_{\text{int}} \tag{17}$$

$$R_{\text{int}} = \frac{r_{mem} L}{A_{cell}} \tag{18}$$

$$r_{mem} = \frac{181.6\left[1 + 0.03 i + 0.062\left(\frac{T_{fc}}{303}\right)^2 i^{2.5}\right]}{\left(\psi - 0.634 - 3i\right)\exp\left(4.18\left(T_{fc} - 303\right)/T_{fc}\right)} \tag{19}$$

where R_{int}, r_{mem} and ψ represent the total internal resistance, membrane resistivity, and membrane water content, respectively. The concentration overpotential arises due to the concentration gradient between the reactants or products at the electrode surface and the solution and is expressed as follows:

$$V_{conc} = \frac{RT_{fc}}{n_e F}\ln\left(\frac{i_L}{i_L - i}\right) \tag{20}$$

where i_L is the current density. The overall amount of heat generated in the fuel cell can be calculated through the energy equation in the fuel cell.

$$\dot{Q}_{net} = \dot{Q}_{ch} - W_{fc} - \dot{Q}_{s,l} \tag{21}$$

$$\dot{Q}_{ch} = \dot{n}_{H_2,cons} HHV \tag{22}$$

where $\dot{Q}_{ch}$ and $\dot{Q}_{s,l}$ are the chemical energy and the sensible and latent heat. HHV is the higher heating value of hydrogen. The

consumption rate of the hydrogen, oxygen, and production rate of water can be calculated as:

$$\dot{n}_{H_2,cons} = N_{cell}\frac{I}{2F} \tag{23}$$

$$\dot{n}_{O_2,cons} = N_{cell}\frac{I}{4F} \tag{24}$$

Moreover, the hydrogen and oxygen molar flow rates can be determined as:

$$\dot{n}_{H_2} = \lambda_{H_2}\dot{n}_{H_2,cons} = \lambda_{H_2}N_{cell}\frac{I}{2F} \tag{25}$$

$$\dot{n}_{O_2} = \lambda_{O_2}\dot{n}_{O_2,cons} = \lambda_{H_2}N_{cell}\frac{I}{4F} \tag{26}$$

The sensible and latent heat can be calculated by:

$$\begin{aligned}\dot{Q}_{s,l} = {} & C_{p,H2}\left(\dot{n}_{H_2,out}T_{fc} - \dot{n}_{H_2,in}T_{in}\right) + \\ & C_{p,O_2}\left(\dot{n}_{O_2,out}T_{fc} - \dot{n}_{O_2,in}T_{in}\right) + \\ & C_{p,N_2}\left(\dot{n}_{N_2,out}T_{fc} - \dot{n}_{N_2,in}T_{in}\right) + \dot{n}_{H_2O,gen}H_v\end{aligned} \tag{27}$$

Furthermore, compressor electrical power can be calculated as follows:

$$\dot{W}_{comp} = \frac{\dot{m}_{air}\left(k/\left(k-1\right)\right)RT_{amb}\left(\pi^{\left(\frac{k-1}{k}\right)} - 1\right)}{\left(\eta_{comp}\right)} \tag{28}$$

The energy efficiency of the fuel cell is calculated as follows:

$$\eta_{fc} = \frac{\dot{W}_{fc} - \dot{W}_{comp}}{\left(\dot{n}_{H_2,cons}\right).HHV} \tag{29}$$

The generated heat of the fuel cell is delivered to an ORC-EVCR hybrid cycle to produce power and refrigeration. In order to analyze the thermodynamic performance of the system, the mass balance equation, the energy and the exergy equations are applied to all components of the system.

$$\sum \dot{m}_i - \sum \dot{m}_e = 0 \tag{30}$$

$$\sum \dot{m}_i h_i - \sum \dot{m}_e h_e + \sum \dot{Q} - \sum \dot{W} = 0 \tag{31}$$

$$\dot{E}_d = \dot{E}_{in} - \dot{E}_{out} + \dot{E}_Q + \dot{E}_W \tag{32}$$

The exergy of each point of the system can be obtained as follows:

$$ex = ex_{ph} + ex_{ch} \tag{33}$$

where ex_{ph} and ex_{ch} are physical and chemical exergy, respectively, which can be expressed using the following equations:

$$ex_{ph} = \left(h - h_0\right) - T_0\left(s - s_0\right) \tag{34}$$

$$ex_{ch} = \sum x_n ex_{ch,n} + RT_0\sum x_n \ln x_n \tag{35}$$

where x_n is the mole fraction of species n and $ex_{ch,n}$ is the chemical exergy of the species n in dead state. The standard chemical exergies can be found in [42].

The equations for energy and exergy of each component of the system are presented in Table 1.

The efficiency of the ORC-EVCR and the total efficiency of the system can be calculated as follows:

$$COP_s = \frac{\dot{Q}_{evp}}{\dot{Q}_{net} + \dot{W}_{pump}} \tag{36}$$

$$\eta_{total} = \frac{\dot{W}_{fc} - \dot{W}_{comp} + \dot{Q}_{evp}}{\left(\dot{n}_{H_2,cons}\right).HHV + \dot{W}_{pump}} \tag{37}$$

Moreover, the exergy efficiency of the ORC-EVCR, PEM fuel cell, and total system can be obtained through the following equations:

$$\eta_{x,ORC-EVCR} = \frac{\dot{Q}_{evp}\left(1 - \frac{T_0}{T_{evp}}\right)}{\dot{Q}_{net}\left(1 - \frac{T_0}{T_{fc}}\right) + \dot{W}_{pump}} \tag{38}$$

$$\eta_{x,fc} = \frac{\dot{W}_{fc} - \dot{W}_{comp}}{\left(\dot{E}x_{air,in} + \dot{E}x_{H_2,in}\right) - \left(\dot{E}x_{air,out} + \dot{E}x_{H_2O,gen}\right)} \tag{39}$$

$$\eta_{x,total} = \frac{\dot{W}_{fc} - \dot{W}_{comp} + \dot{Q}_{evp}\left(1 - \frac{T_0}{T_{evp}}\right)}{\left(\dot{E}x_{air,in} + \dot{E}x_{H_2,in}\right) - \left(\dot{E}x_{air,out} + \dot{E}x_{H_2O,gen}\right) + \dot{W}_{pump}} \tag{40}$$

4. Result and discussion

In the present study, the thermodynamic performance of an ORC-EVCR system integrated with a PEM fuel cell is analyzed using R290 as the working fluid. Table 2 represents the input parameters used in the thermodynamic modeling. EES software is used to perform all computations.

Table 1. Exergy and exergy cost balance equations for the system components

Component	Energy equation	Exergy equation
Turbine	$\dot{W}_{tur} = \dot{m}_{12}\left(h_{12} - h_{13}\right)$	$\dot{E}x_{12} = \dot{E}x_{13} + \dot{W}_{tur} + \dot{E}_{D,tur}$
Fuel cell	$\dot{Q}_{net} = \dot{m}_{11}\left(h_{12} - h_{11}\right)$	$\dot{E}x_{11} + \dot{E}x_{16} + \dot{E}x_{18} = \dot{E}x_{19} + \dot{E}x_{20} + \dot{E}x_{21} + \dot{E}_{D,fc}$
Condenser	$\dot{Q}_{Cond} = \dot{m}_{14}\left(h_{14} - h_{9}\right)$	$\dot{E}x_{14} + \dot{Q}_{cond}\left(1 - \frac{T_0}{T_{cond}}\right) = \dot{E}x_9 + \dot{E}_{D,Cond}$
Pump	$\dot{W}_{pump} = \dot{m}_{10}\left(P_{11} - P_{10}\right) / \rho\eta_p$ $\dot{W}_{pump} = \dot{m}_{11}h_{11} - \dot{m}_{10}h_{10}$	$\dot{E}x_{10} = \dot{E}x_{11} - \dot{W}_{Pump} + \dot{E}_{D,pump}$
EVCR Compressor	$\dot{W}_{Comp} = \dot{m}_4\left(h_4 - h_5\right)$ $\eta_{comp} = \frac{h_{5s} - h_4}{h_5 - h_4}$	$\dot{E}x_4 + \dot{W}_{Comp} = \dot{E}x_5 + \dot{E}_{D,Comp}$
Ejector	$\eta_p = \frac{h_{p,1} - h_{p,1a}}{h_{p,1} - h_{p,1i}}$ $u_{p,1a} = \sqrt{2\left(h_{p,1} - h_{p,1a}\right)}$ $\eta_s = \frac{h_{s,2} - h_{s,1a}}{h_{s,2} - h_{s,1i}}$ $u_{s,1a} = \sqrt{2\left(h_{s,2} - h_{s,1a}\right)}$ $\dot{m}_1 u_{p,1a} + \dot{m}_2 u_{s,1a} = \dot{m}_3 u_{t,1m}$ $\dot{m}_1\left(h_{p,1a} + \frac{u_{p,1a}^2}{2}\right)u_{p,1a} + \dot{m}_2\left(h_{s,1a} + \frac{u_{s,1a}^2}{2}\right) = \dot{m}_3\left(h_{t,1m} + \frac{u_{t,1m}^2}{2}\right)$ $\eta_d = \frac{h_{3i} - h_{t,1m}}{h_3 - h_{t,1m}}$ $h_{p,1} + \mu h_{s,2} = \left(1 + \mu\right)h_3$ $x_3 = \frac{1}{1 + \mu}$	$\dot{E}x_1 + \dot{E}x_2 = \dot{E}x_3 + \dot{E}_{D,Ejector}$
Separator	$\dot{m}_3 h_3 = \dot{m}_4 h_4 + \dot{m}_6 h_6$	$\dot{E}x_3 = \dot{E}x_4 + \dot{E}x_6 + \dot{E}_{D,Sep}$
Evaporator	$\dot{Q}_{evp} = \dot{m}_7\left(h_8 - h_7\right)$	$\dot{E}x_7 + \dot{Q}_{evp}\left(1 - \frac{T_0}{T_{evp}}\right) = \dot{E}x_8 + \dot{E}_{D,evp}$
Trottling valve	$h_6 = h_7$	$\dot{E}x_6 = \dot{E}x_7 + \dot{E}_{D,V}$

Table 2. The input parameters of the fuel cell [9, 19, 29].

Parameter	Value
Farady Constant	96485 (C/mol)
Number of electrons	2
Number of cells	13000
Limiting current density	1.5 (A/ cm^2)
Stack operating current density	0.6 (A/ cm^2)
Active surface area	232 (cm^2)
Membrane thickness	0.0178 (cm)
Operating temperature of PEM	358.15 (K)
Operating pressure of PEM	3 (bar)
Stoichiometric rate of hydrogen	1.2
Stoichiometric rate of air	2
Vaporization heat of water	40644 J/mol
Specific heat capacity of oxygen	29.72 J/(mol.K)
Specific heat capacity of nitrogen	28.39 J/(mol.K)
Higher heating value of hydrogen	285.55 J/(mol.K)
Specific heat capacity of hydrogen	28.86 J/(mol.K)
Specific heat capacity of water	75.95 J/(mol.K)

The simulation of ORC-VCR is validated while using the data of [35]. The comparison is indicated in Table 3 and it shows good consistency between the main thermodynamic results. In order to validate the numerical modeling of the PEM fuel cell, the fuel cell voltage is compared with the data presented by Ref [9]. As can be observed from Fig.2 there is a good agreement between the current results with those reported by Ref [9]. In Table 4 the value of energy and exergy related parameters of the proposed system and an ORC-VCR system is presented. The results in Table 3 are obtained using the input data given in Table 2. Referring to Table 3, there is an increment of 18.88% in $\dot{Q}_{evp}$, 12.29 % in COP_s, and 12.27% in $\eta_{x,CCP}$ compared to the ORC-VCR system. Moreover, this improvement leads to 2.97 % increase in total system energy efficiency and a 0.64% increase in total system exergy efficiency. Furthermore, the overall energy and exergy efficiency of the system is 33.43% and 5.46% higher than a standalone PEM fuel cell. The exergy destruction rates for each system component are displayed in Fig.3. As can be observed, in the ORC-EVCR system, the condenser has the maximum exergy destruction rate which is about 31% of the total exergy destruction of the system.

Figure 4 displays the effect of evaporator temperature on the thermodynamic performance of the system. As can be observed, as the evaporator temperature rises, the energy efficiency of the cycle increases. This is because, with the rise of the evaporator temperature, the specific enthalpy difference between the evaporator and compressor decreases. Meanwhile, as the input energy from the fuel cell is constant, the compressor work does not change. Hence, the mass flow rate of the refrigeration cycle increases which compensates for the enthalpy difference across the evaporator. Therefore, the refrigeration capacity and system efficiency increase with rising the evaporator temperature. It can be observed from Fig.4b that the increase in evaporator temperature, leads to a decrease in system energy efficiency. As the input exergy to the system remains constant, increasing the mass flow rate of the system leads to higher exergy destruction in the refrigeration components and the exergy efficiency decreases.

Table 3. Comparison of ORC-VCR cycle parameters with Ref [35]

Parameter	Present study	Ref [35]
$\dot{W}_{turbine}$ (kW)	59.57	59.59
$\dot{Q}_{evp}$ (kW)	300.5	301.1
COP_s	0.5886	0.589
η_x (%)	30.45	30.65

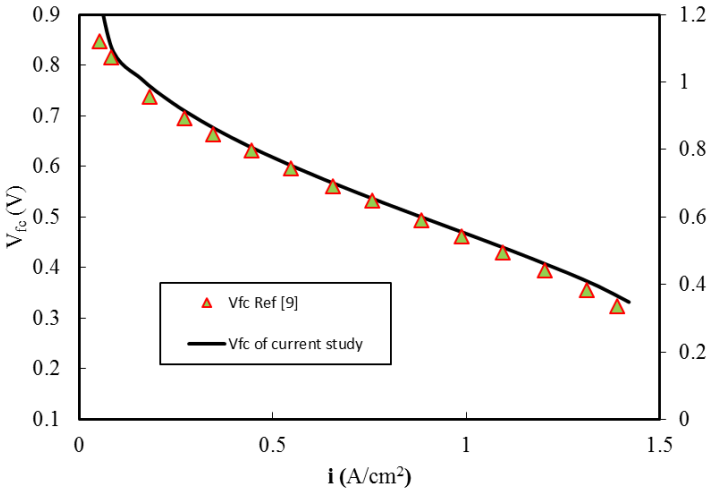

Fig. 2. Fuel cell modeling verification by [9]

Table 4. Result of energy and exergy analysis for PEM-ORC-EVCR and PEM-ORC-VCR system.

Parameter	PEM-ORC-EVCR	PEM-ORC-VCR
$\dot{W}_{turbine}$ (kW)	114.9	114.9
$\dot{W}_{fc}$ (kW)	1058	1058
$\dot{Q}_{evp}$ (kW)	329.3	277
COP_s (%)	25.49	22.7
η_{fc} (%)	32.96	32.96
η_{total} (%)	43.98	42.71
$\eta_{x,CCP}$ (%)	30.27	26.96
$\eta_{x,fc}$ (%)	41.76	41.76
$\eta_{x,total}$ (%)	44.04	43.76
$\dot{I}_{ORC-EVCR}$ (kW)	83.2	89.3

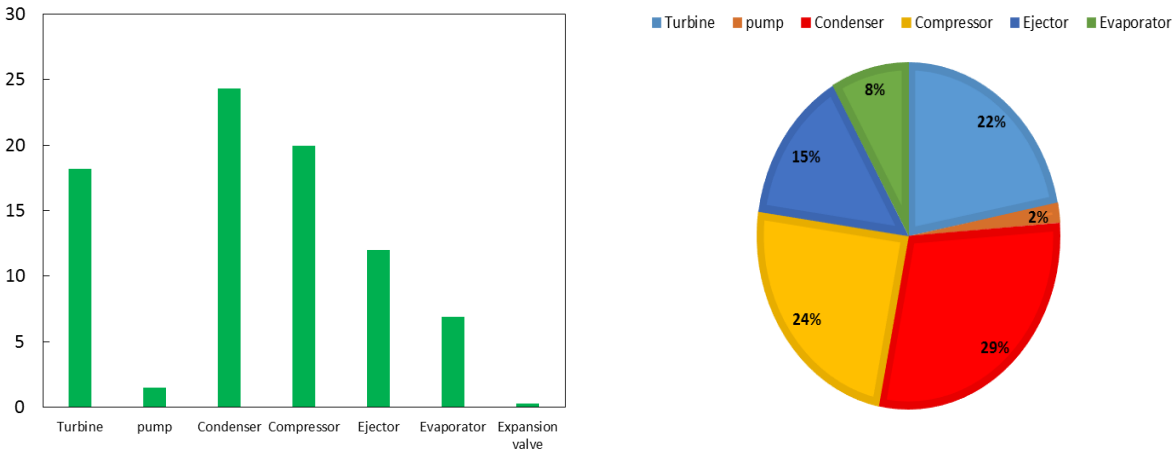

(a) **(b)**

Fig. 3. Exergy destruction rate (a) and proportion (b) for different components of the system.

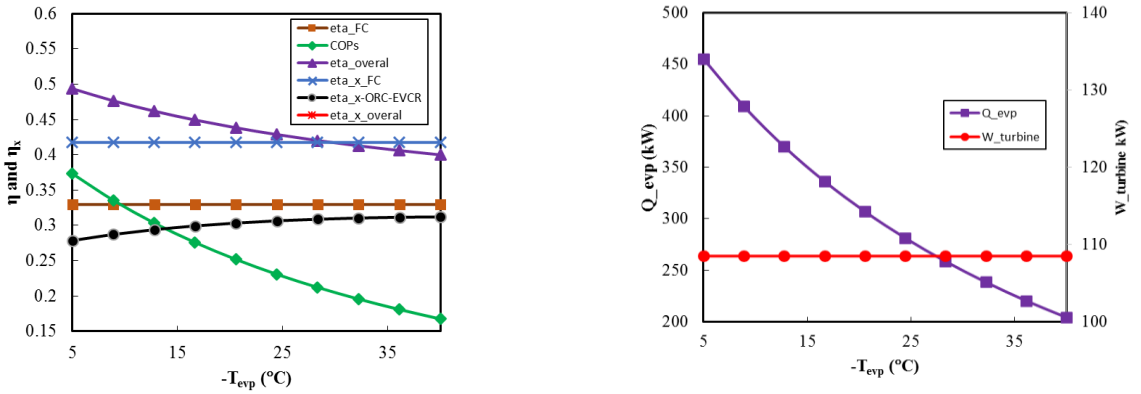

(a) **(b)**

Fig. 4. Effect of Variations of evaporator temperature on a) energy and exergy efficiency, b) refrigeration capacity and turbine work.

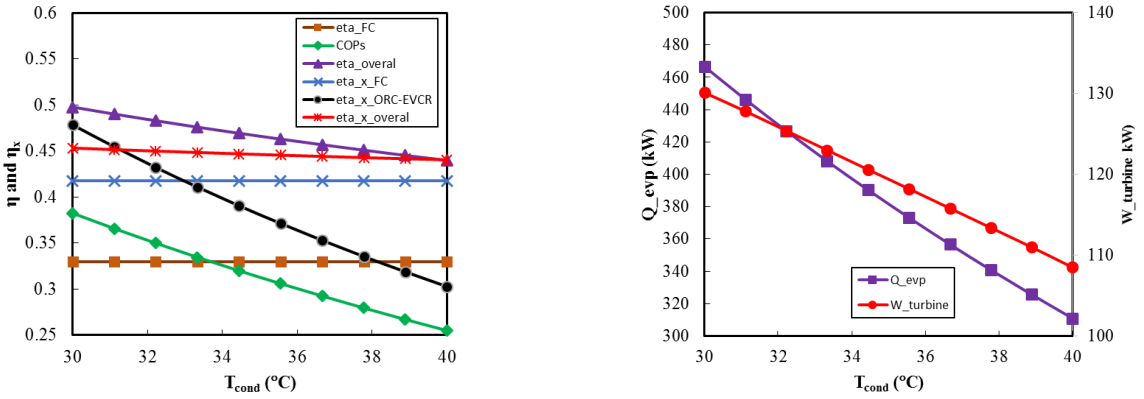

(a) **(b)**

Fig. 5. Effect of Variations of condenser temperature on a) energy and exergy efficiency, b) refrigeration capacity and turbine work.

The effect of the condensation temperature on the thermodynamic performance of the system is indicated in Fig.5. As shown in Fig.5a the COP_s and η_{total} decrease from 0.3823 to 25.49 and from 0.4977 to 0.4398 with increasing the condensation temperature from 30°C to 40°C. As the input energy to the system is constant, rising the condensation temperature leads to an increase in the enthalpy at the turbine exit and the produced work of the turbine decreases. Accordingly, the compressor required power decreases. Furthermore, by increasing the condenser temperature, the enthalpy difference across the compressor increases. The increase in the compressor-specific work and decrease in required compressor work result in a reduction in the mass flow rate of the refrigeration cycle. Hence the cooling capacity of the cycle decreases. Whereas the PEM fuel cell parameters are constant, the reduction in cooling capacity decreases the energy efficiency of the system.

Figure 6 illustrates the effect of fuel cell operating temperature on the thermodynamic performance of the system. As can be seen from Fig.6 a by increasing the fuel cell operating temperature, energy and exergy efficiencies of the PEM fuel cell increase. However, the total energy and exergy efficiencies of the system decrease. This is because as the fuel cell operating temperature increases, the proton exchange rate increases which leads to an increase in the voltage and a decrease in the irreversibilities of the fuel cell. Therefore, the fuel cell output power increases. Moreover, the inlet fuel flow rate doesn't

change which leads to an increase in the energy and exergy efficiencies of the fuel cell. On the other hand, by increasing the fuel cell performance, the heat generated in the fuel cell decreases and lower energy is delivered to the ORC-EVCR. Hence, the specific enthalpy of the ORC fluid exiting the fuel cell decreases. However, the mass flow rate of the ORC increases which results in higher turbine powers. Accordingly, the power of the compressor and the net cooling effect in the evaporator increase. Hence, the total energy and exergy of the system increase.

The effect of the fuel cell operating pressure on the system performance is depicted in Fig. 7. At higher pressures, the mass transport resistance problems and the fuel cell over potentials decrease due to the improvement of the diffusivity of the reactant gases. Therefore, the cell voltage and consequently the output power of the fuel cell increase. Enhancing the fuel cell performance leads to a decrease in heat generation which lowers the delivered energy to the ORC-EVCR system. Therefore, the refrigeration capacity, the compressor work, and the turbine power decrease. However, increasing the fuel cell power is more prominent and the energy efficiency of the system increases. By increasing the fuel cell performance, the exergy destruction in the cell decreases. Furthermore, increasing the fuel cell output power dominates the reduction in refrigeration energy, and the exergy efficiency of the system increases.

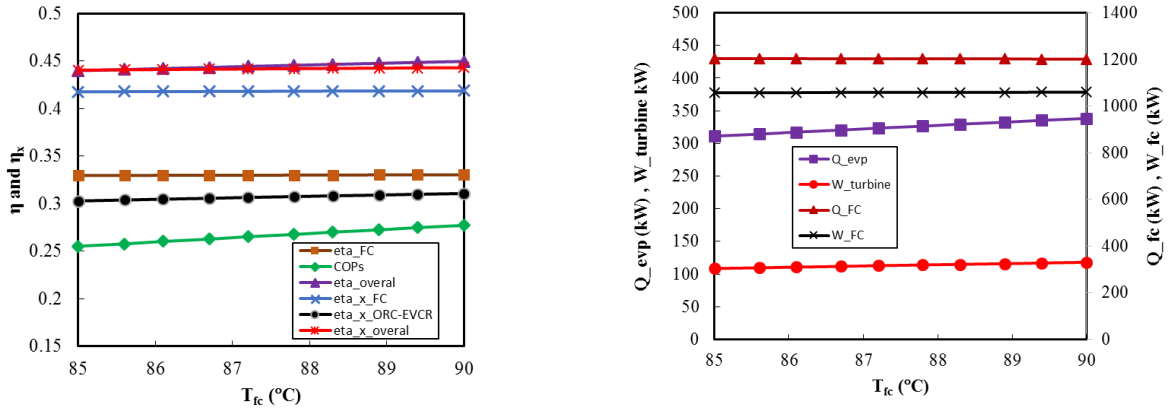

(a) **(b)**

Fig. 6. Effect of Variations of fuel cell temperature on a) energy and exergy efficiency, b) refrigeration capacity, turbine work, fuel cell heat, and fuel cell power

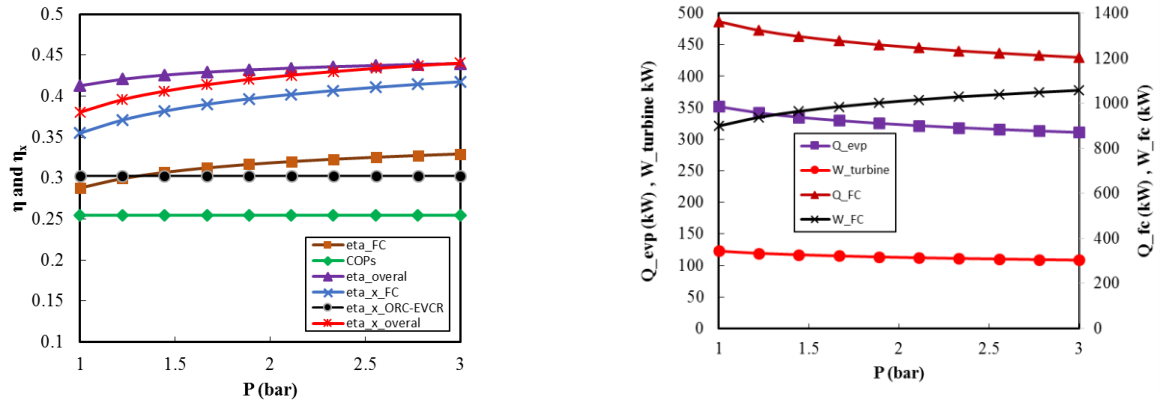

(a) **(b)**

Fig. 7. Effect of Variations of fuel cell operating pressure on a) energy and exergy efficiency, b) refrigeration capacity, turbine work, fuel cell heat, and fuel cell power

The effect of the current density on the energy and exergy efficiencies of the system is illustrated in Fig.8. As can be seen from Fig.4 both efficiencies show a downward trend as the current density rises. This is because with increasing the current density, the fuel cell output power and heat generation increase. Accordingly, more input energy is delivered to the OCR-EVCR system and more cooling capacity can be achieved. On the other hand, as the current density increases, the fuel consumption and the air compressor power also increase which has more influence on the system efficiency. By increasing the current density from 0.1 to 0.6, the $\dot{W}_{fc}$ increases from 247.6 to 1058, the $\dot{Q}_{fc}$ increases from 129.4 to 1204, the $\dot{Q}_{evp}$ increase from 33.42 to 311, and the hydrogen mole consumption increase from 1.563 to 9.377. Furthermore, by increasing the current density, the mass flow rates and irreversibilities like voltage losses increase which results in higher exergy destruction rates. Accordingly, a descending trend can be observed in the energy efficiency and the exergy efficiency of the system.

Figure 9 represents the variation of refrigeration capacity and ejector destruction rate with increasing the ejector efficiencies. As shown in Fig.9.a with increasing the η_{mn} , η_{sn} and η_d from 0.7 to 0.9, the refrigeration capacity increases by 4.28%, 0.87%, and 4.97%, respectively. Moreover, in higher ejector efficiencies, the exergy destruction rate in the ejector decreases. Furthermore, the effect of increasing the diffuser efficiency on reducing the ejector destruction rate is more prominent.

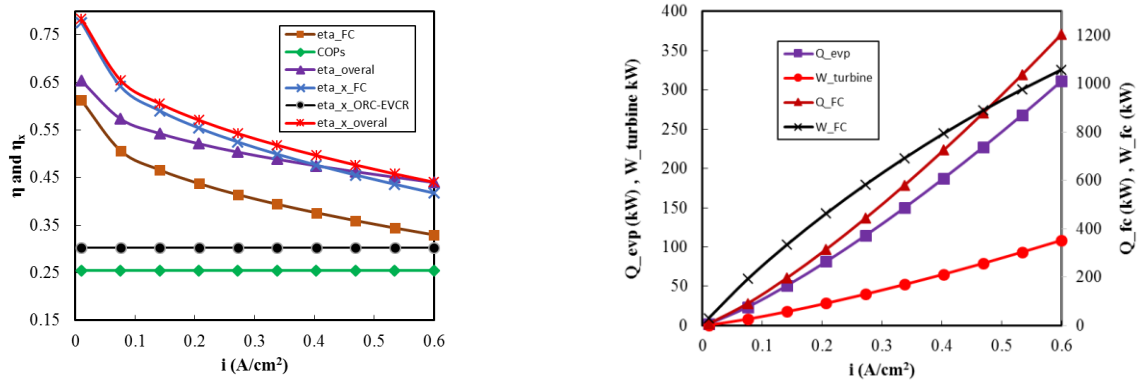

(a) **(b)**

Fig. 8. Effect of Variations of current density on a) energy and exergy efficiency, b) refrigeration capacity, turbine work, fuel cell heat, and fuel cell power

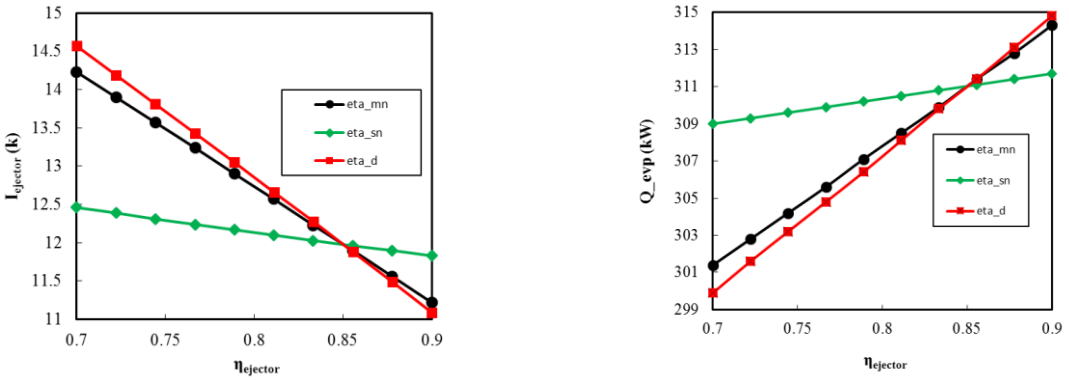

(a) **(b)**

Fig. 9. Effect of Variations of ejector efficiencies on a) ejector exergy destruction rate, b) refrigeration capacity.

5. Conclusion

In this research, a novel hybrid system consisting of a PEM fuel cell and a combined ORC-EVCR system employing an ejector expansion is presented. The waste heat of the PEM fuel cell is delivered to the ORC-EVCR to produce refrigeration. The efficiency of the proposed system is compared to a PEM-ORC-VCR without using the ejector. Moreover, the parametric study is carried out to investigate the effect of important parameters of the two subsystems. The main results of this study can be concluded as follows:

- Using the ejector, the refrigeration capacity, energy efficiency, and exergy efficiency of the ORC-EVCR system increase by 18.88%, 12.29 %, and 12.27%, respectively.
- Compared to the ejector diffuser nozzle, increasing the efficiency of the motive and suction nozzle of the ejector has a more prominent effect on refrigeration capacity.
- The overall energy and exergy efficiency of the system is 33.43% and 5.46% higher than a standalone PEM fuel cell.
- In lower evaporator temperatures, the exergy efficiency of the ORC-EVCR system increases. However, the energy efficiency of this system increases at higher evaporator temperatures.
- Increasing the condenser temperature leads to a decrease in the energy and exergy efficiencies of the ORC-EVCR system.
- By increasing the PEM fuel cell operating temperature, the generated power of the fuel cell increases, and the rejected waste heat of the fuel cell decreases. However the refrigeration capacity and overall efficiency of the system increase.
- In higher current densities of the fuel cell, a descending trend can be observed in the energy efficiency and the exergy efficiency of the system.
- By increasing the fuel cell operating pressure, the proposed system reaches higher energy and exergy efficiency.

References

[1] A. Anderson, B. Rezaie, Geothermal technology: Trends and potential role in a sustainable future, Applied Energy, Vol. 248, pp. 18-34, 2019/08/15/, 2019.

[2] X. Cheng, Z. Shi, N. Glass, L. Zhang, J. Zhang, D. Song, Z.-S. Liu, H. Wang, J. Shen, A review of PEM hydrogen fuel cell contamination: Impacts, mechanisms, and mitigation, Journal of Power Sources, Vol. 165, No. 2, pp. 739-756, 2007/03/20/, 2007.

[3] V. Mehta, J. S. Cooper, Review and analysis of PEM fuel cell design and manufacturing, Journal of Power Sources, Vol. 114, No. 1, pp. 32-53, 2003/02/25/, 2003.

[4] O. Bamisile, Q. Huang, M. Dagbasi, V. Adebayo, E. C. Okonkwo, P. Ayambire, T. Al-Ansari, T. A. H. Ratlamwala, Thermo-environ study of a concentrated photovoltaic thermal system integrated with Kalina cycle for multigeneration and hydrogen production, International Journal of Hydrogen Energy, Vol. 45, No. 51, pp. 26716-26732, 2020/10/16/, 2020.

[5] G. Besagni, R. Mereu, F. Inzoli, Ejector refrigeration: A comprehensive review, Renewable and Sustainable Energy Reviews, Vol. 53, pp. 373-407, 2016/01/01/, 2016.

[6] K. Sumeru, H. Nasution, F. N. Ani, A review on two-phase ejector as an expansion device in vapor compression refrigeration cycle, Renewable and Sustainable Energy Reviews, Vol. 16, No. 7, pp. 4927-4937, 2012/09/01/, 2012.

[7] N. Zhang, N. Lior, Development of a Novel Combined Absorption Cycle for Power Generation and Refrigeration, Journal of Energy Resources Technology, Vol. 129, No. 3, pp. 254-265, 2006.

[8] P. Srikhirin, S. Aphornratana, S. Chungpaibulpatana, A review of absorption refrigeration technologies, Renewable and Sustainable Energy Reviews, Vol. 5, No. 4, pp. 343-372, 2001/12/01/, 2001.

[9] M. H. Ahmadi, A. Mohammadi, F. Pourfayaz, M. Mehrpooya, M. Bidi, A. Valero, S. Uson, Thermodynamic analysis and optimization of a waste heat recovery system for proton exchange membrane fuel

cell using transcritical carbon dioxide cycle and cold energy of liquefied natural gas, Journal of Natural Gas Science and Engineering, Vol. 34, pp. 428-438, 2016/08/01/, 2016.

[10] S. Authayanun, V. Hacker, Energy and exergy analyses of a stand-alone HT-PEMFC based trigeneration system for residential applications, Energy Conversion and Management, Vol. 160, pp. 230-242, 2018/03/15/, 2018.

[11] A. Azad, I. Fakhari, P. Ahmadi, N. Javani, Analysis and optimization of a fuel cell integrated with series two-stage organic Rankine cycle with zeotropic mixtures, International Journal of Hydrogen Energy, Vol. 47, No. 5, pp. 3449-3472, 2022/01/15/, 2022.

[12] M. Chahartaghi, B. A. Kharkeshi, Performance analysis of a combined cooling, heating and power system with PEM fuel cell as a prime mover, Applied Thermal Engineering, Vol. 128, pp. 805-817, 2018/01/05/, 2018.

[13] I. Fakhari, A. Behzadi, E. Gholamian, P. Ahmadi, A. Arabkoohsar, Comparative double and integer optimization of low-grade heat recovery from PEM fuel cells employing an organic Rankine cycle with zeotropic mixtures, Energy Conversion and Management, Vol. 228, pp. 113695, 2021/01/15/, 2021.

[14] X. Guo, H. Zhang, J. Zhao, F. Wang, J. Wang, H. Miao, J. Yuan, Performance evaluation of an integrated high-temperature proton exchange membrane fuel cell and absorption cycle system for power and heating/cooling cogeneration, Energy Conversion and Management, Vol. 181, pp. 292-301, 2019/02/01/, 2019.

[15] M. Hasani, N. Rahbar, Application of thermoelectric cooler as a power generator in waste heat recovery from a PEM fuel cell – An experimental study, International Journal of Hydrogen Energy, Vol. 40, No. 43, pp. 15040-15051, 2015/11/16/, 2015.

[16] S. Kaushik A, S. S. Bhogilla, P. Muthukumar, Thermal integration of Proton Exchange Membrane Fuel Cell with recuperative organic rankine cycle, International Journal of Hydrogen Energy, Vol. 46, No. 27, pp. 14748-14756, 2021/04/19/, 2021.

[17] S. Khanmohammadi, M. Saadat-Targhi, Thermodynamic and economic assessment of an integrated thermoelectric generator and the liquefied natural gas production process, Energy Conversion and Management, Vol. 185, pp. 603-610, 2019/04/01/, 2019.

[18] M. Z. Malik, F. Musharavati, S. Khanmohammadi, A. H. Pakseresht, S. Khanmohammadi, D. D. Nguyen, Design and comparative exergy and exergo-economic analyses of a novel integrated Kalina cycle improved with fuel cell and thermoelectric module, Energy Conversion and Management, Vol. 220, pp. 113081, 2020/09/15/, 2020.

[19] S. Marandi, F. Mohammadkhani, M. Yari, An efficient auxiliary power generation system for exploiting hydrogen boil-off gas (BOG) cold exergy based on PEM fuel cell and two-stage ORC: Thermodynamic and exergoeconomic viewpoints, Energy Conversion and Management, Vol. 195, pp. 502-518, 2019/09/01/, 2019.

[20] S. Marandi, N. Sarabchi, M. Yari, Exergy and exergoeconomic comparison between multiple novel combined systems based on proton exchange membrane fuel cells integrated with organic Rankine cycles, and hydrogen boil-off gas subsystem, Energy Conversion and Management, Vol. 244, pp. 114532, 2021/09/15/, 2021.

[21] H. Montazerinejad, E. Fakhimi, S. Ghandehariun, P. Ahmadi, Advanced exergy analysis of a PEM fuel cell with hydrogen energy storage integrated with organic Rankine cycle for electricity generation, Sustainable Energy Technologies and Assessments, Vol. 51, pp. 101885, 2022/06/01/, 2022.

[22] H. Q. Nguyen, B. Shabani, Proton exchange membrane fuel cells heat recovery opportunities for combined heating/cooling and power applications, Energy Conversion and Management, Vol. 204, pp. 112328, 2020/01/15/, 2020.

[23] T. Özgür, A. C. Yakaryilmaz, Thermodynamic analysis of a Proton Exchange Membrane fuel cell, International

Journal of Hydrogen Energy, Vol. 43, No. 38, pp. 18007-18013, 2018/09/20/, 2018.

[24] V. Rezaee, A. Houshmand, Energy and Exergy Analysis of a Combined Power Generation System Using PEM Fuel Cell and Kalina Cycle System 11, Periodica Polytechnica Chemical Engineering, Vol. 60, pp. 98-105, 03/25, 2016.

[25] N. Sarabchi, S. M. S. Mahmoudi, M. Yari, A. Farzi, Exergoeconomic analysis and optimization of a novel hybrid cogeneration system: High-temperature proton exchange membrane fuel cell/Kalina cycle, driven by solar energy, Energy Conversion and Management, Vol. 190, pp. 14-33, 2019/06/15/, 2019.

[26] S. M. Seyed Mahmoudi, N. Sarabchi, M. Yari, M. A. Rosen, Exergy and Exergoeconomic Analyses of a Combined Power Producing System including a Proton Exchange Membrane Fuel Cell and an Organic Rankine Cycle, Sustainability, Vol. 11, No. 12, 2019.

[27] B. Shabani, J. Andrews, An experimental investigation of a PEM fuel cell to supply both heat and power in a solar-hydrogen RAPS system, International Journal of Hydrogen Energy, Vol. 36, No. 9, pp. 5442-5452, 2011/05/01/, 2011.

[28] S. Toghyani, E. Afshari, E. Baniasadi, Performance evaluation of an integrated proton exchange membrane fuel cell system with ejector absorption refrigeration cycle, Energy Conversion and Management, Vol. 185, pp. 666-677, 2019/04/01/, 2019.

[29] P. Zhao, J. Wang, L. Gao, Y. Dai, Parametric analysis of a hybrid power system using organic Rankine cycle to recover waste heat from proton exchange membrane fuel cell, International Journal of Hydrogen Energy, Vol. 37, No. 4, pp. 3382-3391, 2012/02/01/, 2012.

[30] S. Aphornratana, T. Sriveerakul, Analysis of a combined Rankine–vapour–compression refrigeration cycle, Energy Conversion and Management, Vol. 51, No. 12, pp. 2557-2564, 2010/12/01/, 2010.

[31] H. Wang, R. Peterson, K. Harada, E. Miller, R. Ingram-Goble, L. Fisher, J. Yih, C. Ward, Performance of a combined organic Rankine cycle and vapor compression cycle for heat activated cooling, Energy, Vol. 36, No. 1, pp. 447-458, 2011/01/01/, 2011.

[32] H. Li, X. Bu, L. Wang, Z. Long, Y. Lian, Hydrocarbon working fluids for a Rankine cycle powered vapor compression refrigeration system using low-grade thermal energy, Energy and Buildings, Vol. 65, pp. 167-172, 2013/10/01/, 2013.

[33] Y.-R. Li, X.-Q. Wang, X.-P. Li, J.-N. Wang, Performance analysis of a novel power/refrigerating combined-system driven by the low-grade waste heat using different refrigerants, Energy, Vol. 73, pp. 543-553, 2014/08/14/, 2014.

[34] B. Saleh, Parametric and working fluid analysis of a combined organic Rankine-vapor compression refrigeration system activated by low-grade thermal energy, Journal of Advanced Research, Vol. 7, No. 5, pp. 651-660, 2016/09/01/, 2016.

[35] B. Saleh, Energy and exergy analysis of an integrated organic Rankine cycle-vapor compression refrigeration system, Applied Thermal Engineering, Vol. 141, pp. 697-710, 2018/08/01/, 2018.

[36] N. Zheng, J. Wei, L. Zhao, Analysis of a solar Rankine cycle powered refrigerator with zeotropic mixtures, Solar Energy, Vol. 162, pp. 57-66, 2018/03/01/, 2018.

[37] Ashwni, A. F. Sherwani, D. Tiwari, Thermodynamic analysis of simple and modified organic Rankine cycle and vapor compression refrigeration (ORC–VCR) systems, Environmental Progress & Sustainable Energy, Vol. 40, No. 3, pp. e13577, 2021/05/01, 2021.

[38] J. Bao, L. Zhang, C. Song, N. Zhang, X. Zhang, G. He, Comparative study of combined organic Rankine cycle and vapor compression cycle for refrigeration: Single fluid or dual fluid?, Sustainable Energy Technologies and Assessments, Vol. 37, pp. 100595, 2020/02/01/, 2020.

[39] T. Ghorbani, M. Yari, F. Mohammadkhani, Thermodynamic Analysis and Feasibility Study of Internal Combustion Engine Waste Heat Recovery to Run its Refrigeration System, AUT Journal of Mechanical Engineering, Vol. 2, No. 2, pp. 253-262, 2018. en

[40] S. Karellas, K. Braimakis, Energy–exergy analysis and economic investigation

of a cogeneration and trigeneration ORC–VCC hybrid system utilizing biomass fuel and solar power, Energy Conversion and Management, Vol. 107, pp. 103-113, 2016/01/01/, 2016.

[41] K. H. Kim, H. Perez-Blanco, Performance analysis of a combined organic Rankine cycle and vapor compression cycle for power and refrigeration cogeneration, Applied Thermal Engineering, Vol. 91, pp. 964-974, 2015/12/05/, 2015.

[42] J. Szargut, 2005, Exergy Method: Technical and Ecological Applications, WIT Press